

M_F -dependent hyperfine-induced $5s5p\ ^3P_0^o-5s^2\ ^1S_0$ clock transition rates in an external magnetic field for ^{87}Sr

Xiaotong Lu^{⊗,1}, Feng Guo,¹ Yebing Wang^{⊗,1}, Min Feng,¹ Ting Liang,¹ Benquan Lu^{⊗,1,*} and Hong Chang^{1,2,†}

¹National Time Service Center, Xi'an 710000, China

²School of Astronomy and Space Science, The University of Chinese Academy of Sciences, Beijing 100088, China

 (Received 23 May 2023; accepted 7 July 2023; published 28 July 2023; corrected 26 September 2023)

In this paper, we theoretically calculate the natural lifetime of the $5s5p\ ^3P_0^o$ state of the ^{87}Sr atom and evaluate the effect of an external magnetic field on the lifetimes of Zeeman sublevels. Using the multiconfiguration Dirac-Hartree-Fock method, the hyperfine-induced $5s5p\ ^3P_0^o-5s^2\ ^1S_0$ clock transition rate of ^{87}Sr is estimated as $6.39(37) \times 10^{-3}\ \text{s}^{-1}$, corresponding to a lifetime of 156(9) s. Our result closely agrees with previous measurements after correcting the decay rate due to the black-body radiation effect. Additionally, the transition rates of Zeeman sublevels are calculated as a function of the magnetic-field strength. Our theoretical results reveal that transition rates between different excited Zeeman states are discrepant, and the lifetime of magnetic sublevel $+M_F^e$ ($-M_F^e$; the superscript e refers to the excited state, i.e., the $5s5p\ ^3P_0^o$ state) will increase (decrease) with the magnetic-field strength. Moreover, we measure the coupling strength between the clock laser and the ^{87}Sr atoms, and our findings align well with theoretical estimations regarding changes in normalized coupling strength with external magnetic-field strength.

DOI: [10.1103/PhysRevA.108.012820](https://doi.org/10.1103/PhysRevA.108.012820)

I. INTRODUCTION

Forbidden transitions with long lifetimes play a critical role in quantum sciences and precision measurements [1–5]. Alkaline-earth-like atoms exhibit an important example of these transitions with the $nsnp\ ^3P_0^o-ns^2\ ^1S_0$ transition. This transition offers a stable and precise frequency reference, making it a key ingredient of optical clocks. State-of-the-art optical clocks based on alkaline-earth-like atoms recently realized an uncertainty of 1.4×10^{-18} [6] and instability of $4.8 \times 10^{-17}\ (\tau/\text{s})^{-0.5}$ [7]. These optical clocks not only can improve the precision of the second in the International System of Units [8–10] but also provide a powerful tool for fundamental physics, including tests of the relativity [11,12], constraints on the ultralight dark matter [13], searches for new physics beyond the standard model [14–16], precise measurements of atomic parameters [17], and studying $SU(N)$ -symmetric many-body interactions [18]. A thorough understanding of the properties of the $nsnp\ ^3P_0^o-ns^2\ ^1S_0$ transition can aid us in comprehending atomic structure and can further improve the performance of optical clocks and other quantum applications.

In odd isotopes of alkaline-earth-like ions or atoms, the $nsnp\ ^3P_0^o-ns^2\ ^1S_0\ E1$ forbidden transition is induced by the hyperfine interaction, which is called the hyperfine-induced transition (HIT) [19–22]. Using the HIT theory, one can estimate the natural lifetime of the $nsnp\ ^3P_0^o$ state and diagnose isotope compositions for extremely low density plasmas [23]. However, we are still uncertain about the exact value of the $^3P_0^o$ -state lifetime of some atoms, such as the ^{87}Sr atom. Although many theoretical studies have been conducted to

determine the lifetime of the $5s5p\ ^3P_0^o$ state in ^{87}Sr , these theoretical values remain roughly consistent (and sometimes inconsistent) with each other while exhibiting large uncertainties [24–27]. In experiment, Dörscher *et al.* [28] reported the decay rate of the $^3P_0^o$ excited state as $\Gamma_0 = 5.2(12) \times 10^{-3}\ \text{s}^{-1}$, which corresponds to a lifetime of 192(44) s. But atoms in the $^3P_0^o$ state can be influenced by black-body radiation (BBR) photons and pumped to the $5s4d\ ^3D_1$ state, subsequently decaying to the ground state via the $^3P_1^o$ state. This process greatly increases the $^3P_0^o$ -state lifetime. After the BBR-induced decay rate was carefully estimated and removed, the natural lifetime of the $^3P_0^o$ state was determined to be 330(140) s. More recently, Muniz *et al.* [29] also determined the $^3P_0^o$ -state lifetime $\tau = 118\ \text{s}$ of ^{87}Sr with a smaller uncertainty of 3 s. However, they neglected to evaluate the BBR-induced transition effect. The two measurements are inconsistent within their uncertainties even though both results account for the BBR-induced decay corrections. Furthermore, it is unclear whether the external magnetic field will influence the HIT rate as there are non-negligible discrepancies between theoretical calculations and experimental measurements in the presence of an external magnetic field for some ions, such as $^{33}\text{S}^{12+}$ [30–33] and $^{47}\text{Ti}^{18+}$ [30,31,33–35]. To explain these experimental and theoretical differences in $^{47}\text{Ti}^{18+}$, Li *et al.* [36] considered the magnetic-field effects on the HIT rate. For alkaline-earth-like atoms and monovalent ions, the effect of the external magnetic field on the quenching rate of the $^3P_0^o$ state, especially its Zeeman sublevels, has not been estimated. In terms of optical clocks, the $^3P_0^o, M_F^e = \pm F$ to $^1S_0, M_F^g = \pm F$ transitions are typically used as the frequency reference to lock the clock laser [6,37–39].

In this work, we calculate the lifetime of the $5s5p\ ^3P_0^o$ clock state in ^{87}Sr by using the multiconfiguration Dirac-Hartree-Fock (MCDHF) method. Our result is in close

*lubenquan@ntsc.ac.cn

†changhong@ntsc.ac.cn

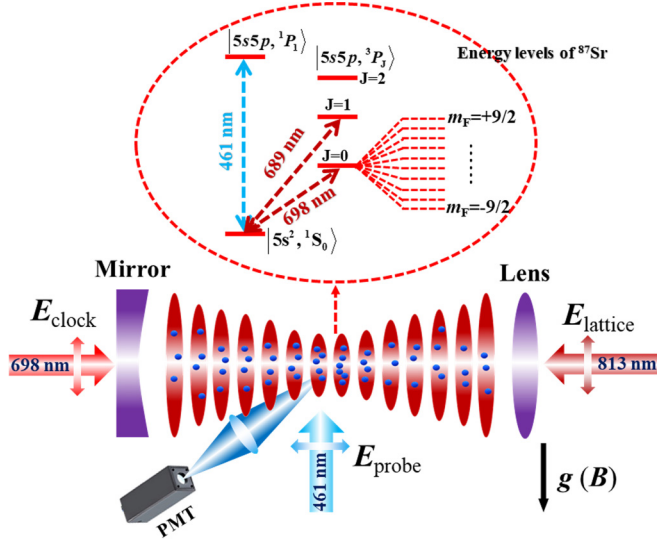


FIG. 1. The experimental setup for the optical lattice and clock transition detection. The optical lattice is produced through the interference between the incident lattice laser beam (813 nm) and its reflector. The clock laser (698 nm) is in alignment with the lattice laser, while both lasers are polarized parallel to the direction of gravity and the magnetic field B , which defines the quantization axis. To collect fluorescence after a 461-nm probe laser pulse, a photomultiplier tube (PMT) is utilized. In the illustration, the energy levels of ^{87}Sr for the clock transition and two stages of laser cooling are depicted.

agreement with the measurements with the correction of the BBR-induced decay rate. Additionally, the external magnetic-field effect on the transition rates between the excited Zeeman states and ground Zeeman states is also estimated. We find that the weak external magnetic field can significantly affect the lifetime of the Zeeman sublevels. Based on the ^{87}Sr optical lattice clock, this result is precisely verified in experiment by measuring the coupling strength between the laser and atoms as a function of the external magnetic-field strength.

II. EXPERIMENTAL MEASUREMENT OF THE RABI FREQUENCY OF THE $5s5p\ ^3P_0^e - 5s^2\ ^1S_0$ CLOCK TRANSITION IN ^{87}Sr

The details of the experimental setup are described elsewhere [40,41]; here we introduce the important experimental processes and parameters for reference. Figure 1 shows the energy levels of ^{87}Sr and the optical lattice and clock-transition-detection equipment. After two stages of laser cooling through the $^1S_0, F^g = 9/2$ to $^3P_1, F' = 9/2, 11/2$ transitions, about 10^6 atoms are trapped and cooled to 3 μK . Next, these atoms are loaded into a one-dimensional optical lattice by turning off all cooling light while keeping the lattice light on permanently. The frequency of the lattice laser is 368 554 485.0(1) MHz, which is stabilized to an ultralow-expansion (ULE) cavity with a fineness of 20 000 [41]. At this “magic frequency,” the lattice ac Stark shift is almost zero. To suppress the tunneling effect, the trap depth is set to $110 E_R$, where E_R represents the recoil energy of the lattice light, as determined from the sideband spectrum [42]. The

initial state is prepared on $^1S_0, M_F^g = -9/2(+9/2)$ using the optical-pumping technique via left-handed or right-handed circularly polarized light at 689 nm (corresponding to the $^1S_0, F^g = 9/2$ to $^3P_1, F' = 9/2$ transition).

To suppress stray magnetic fields around the atoms, we utilized three pairs of Helmholtz coils. The bias magnetic field, which defines the quantization axis along the vertical direction, was generated by the coils used for the magneto-optical trap (MOT). During the laser cooling stage, the MOT coils were configured as anti-Helmholtz and switched to Helmholtz after completing the spin-polarization process. By adjusting the coil current, the magnetic-field strength can be varied from 0 to 200 G.

The $^3P_0^e, F^e = 9/2, M_F^e = \pm 9/2$ to $^1S_0, F^g = 9/2, M_F^g = \pm 9/2$ clock transitions at 698 nm are detected using the clock laser. To achieve an accurate measurement, the flicker-noise floor of the clock laser is reduced to 4×10^{-16} by stabilizing its phase to a ULE cavity with a fineness of 300 000. After the clock laser interacts with the atoms, three probe light pulses of 461 nm are used to determine the populations in the ground state (N_g), excited state (N_e), and background noise (N_b), respectively. The excitation fraction is represented by $(N_e - N_b)/(N_e + N_g - 2N_b)$. The effective coupling strength between the clock laser and atoms is indicated by the oscillation frequency of the Rabi oscillation that shows the excitation fraction of zero detuning as a function of interrogation time. When the clock laser intensity remains constant, the effective coupling strength is determined by the spontaneous radiation lifetime of the excited state. If the bias magnetic-field strength can change the spontaneous radiation lifetime of a specific Zeeman level, the corresponding effective coupling strength will also change. Figure 2 shows the Rabi oscillations for $M_F^e = \pm 9/2$ to $M_F^g = \pm 9/2$ at bias magnetic-field strengths of 2.18 and 199.86 G, respectively. The magnetic-field strength is inferred from the frequency gap between transitions with an uncertainty below 0.6% according to a coefficient of 975.6(36) Hz/G [17,25]. The maximum excitation fractions between Figs. 2(a) and 2(b) differ because the spin-polarized efficiency between $M_F^e = +9/2$ and $M_F^e = -9/2$ is inconsistent. However, this difference does not affect our results because we focus on only the effective coupling strength.

III. INTERNAL AND EXTERNAL MAGNETIC-FIELD EFFECTS ON THE $5s5p\ ^3P_0^e - 5s^2\ ^1S_0$ E1 FORBIDDEN TRANSITION

A. Theory

In the presence of an external magnetic field, the total Hamiltonian of an atom with nonzero nuclear spin I is

$$H = H_{\text{fs}} + H_{\text{hfs}} + H_m. \quad (1)$$

Here H_{fs} is the relativistic fine-structure Hamiltonian, and H_{hfs} is the hyperfine interaction Hamiltonian, which is often given as

$$H_{\text{hfs}} = \sum_k \mathbf{T}^{(k)} \cdot \mathbf{M}^{(k)}, \quad (2)$$

where $\mathbf{T}^{(k)}$ and $\mathbf{M}^{(k)}$ are spherical tensor operators of rank k in the electronic and nuclear spaces [43], respectively. The

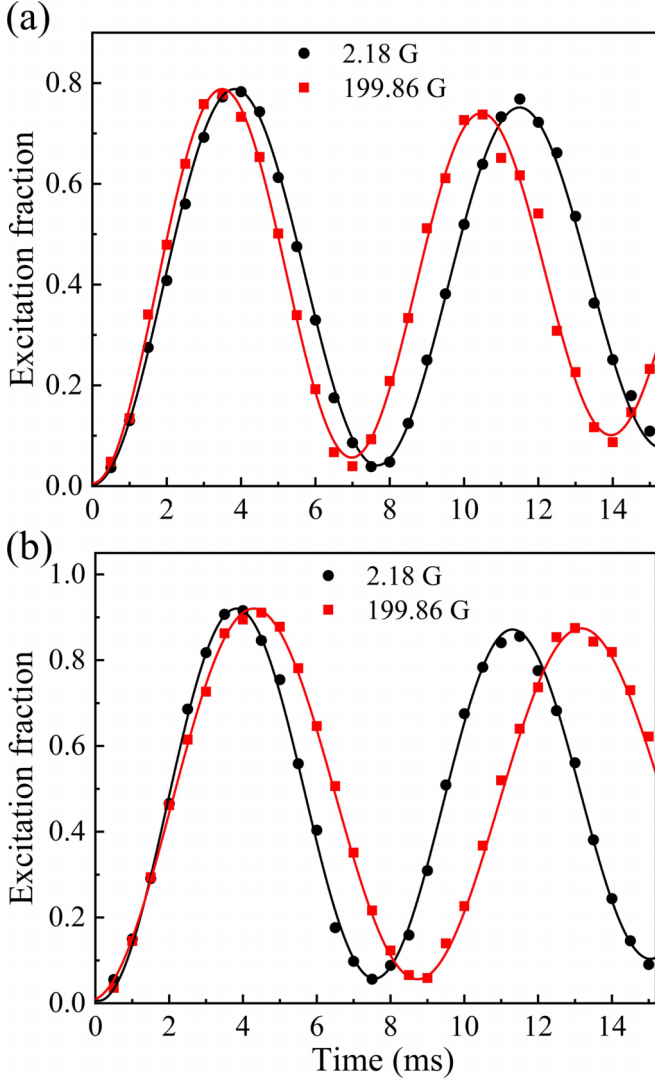


FIG. 2. The Rabi oscillations at different magnetic-field strengths. (a) The ${}^3P_0^e, F^e = 9/2, M_F^e = -9/2$ to ${}^1S_0, F^g = 9/2, M_F^g = -9/2$ transition. At a magnetic-field strength of 2.18 G, the effective coupling strength is 170.2(5) Hz, while at a magnetic-field strength of 199.86 G, the effective coupling strength is 189.2(9) Hz. (b) The ${}^3P_0^e, F^e = 9/2, M_F^e = 9/2$ to ${}^1S_0, F^g = 9/2, M_F^g = 9/2$ transition. The effective coupling strengths are 169.4(6) and 150.3(8) Hz at magnetic-field strengths of 2.18 and 199.86 G, respectively. The solid lines show the fitting using the sinusoidal function with an amplitude that is subject to exponential attenuation.

hyperfine interaction couples the nuclear spin \mathbf{I} and the total electronic angular momentum \mathbf{J} and produces a total angular momentum $\mathbf{F} = \mathbf{I} + \mathbf{J}$. In addition, the hyperfine interaction induces atomic states with different quantum numbers J and opens up new decay channels for some transitions. In Eq. (1), H_m denotes the interaction Hamiltonian between the external magnetic field and the atom, which can be described as [44]

$$H_m = (\mathbf{N}^{(1)} + \Delta\mathbf{N}^{(1)}) \cdot \mathbf{B}. \quad (3)$$

Here $\mathbf{N}^{(1)}$ is a first-order tensor operator that resembles $\mathbf{T}^{(1)}$, but with a difference in the radial part, while $\Delta\mathbf{N}^{(1)}$ represents

the Schwinger quantum electrodynamics (QED) correction [44]. \mathbf{B} denotes the external magnetic field. As the external magnetic field defines the quantization axis, only the magnetic quantum number M_F is a good quantum number. It is worth noting that the external magnetic field can also induce state mixing. According to the theory of the unexpected transition [19–22,36], the atomic wave function can be written as

$$|\gamma\Gamma I J F M_F\rangle = \sum_{\Gamma' J' F'} d_{\Gamma' J' F'} |\gamma\Gamma I J' F' M_F\rangle, \quad (4)$$

where γ and Γ are the other quantum numbers to uniquely describe the nuclear and electronic states. In first-order perturbation theory, the mixing coefficients are given by

$$d_{\Gamma' J' F'} = \frac{\langle \gamma\Gamma I J' F' M_F | H_{\text{hfs}} + H_m | \gamma\Gamma I J F M_F \rangle}{E(\gamma\Gamma I J F M_F) - E(\gamma\Gamma I J' F' M_F)}, \quad (5)$$

where $|\gamma\Gamma I J' F' M_F\rangle$ stands for the perturbing states.

Assuming the external magnetic field is weak, the $5s5p$ ${}^3P_0^e$ -state wave function of ${}^{87}\text{Sr}$ can be expressed as

$$\begin{aligned} |{}^3P_0^e, F^e = 9/2, M_F^e = 9/2\rangle &= |5s5p {}^3P_0^e IF^e = IM_F^e\rangle \\ &+ \sum_{s=1,3; F'} d_{s;F'} |5s5p {}^sP_0^e IF^e = IM_F^e\rangle. \end{aligned} \quad (6)$$

The state within the quotation marks describes the dominant component of the eigenvector. Other interactions from different configurations can be disregarded due to their large energy separations and weak hyperfine and magnetic interactions. To accurately calculate the transition rate, we considered perturbing states with both the same ($\Delta F = 0$) and different ($\Delta F = 1$) total magnetic interactions.

Similarly, the ground-state wave function is given as

$$|{}^1S_0, F^g = 9/2, M_F^g = 9/2\rangle = |5s^2 {}^1S_0 IF^g = IM_F^g\rangle. \quad (7)$$

The one-photon $5s5p$ ${}^3P_0^e$ - $5s^2$ 1S_0 $E1$ transition becomes allowed via mixing with the $5s5p$ ${}^3P_1^e$ and $5s5p$ ${}^1P_1^e$ perturbing states. The transition rate between the excited state $|{}^3P_0^e, F^e = 9/2, M_F^e = 9/2\rangle$ and the ground state $|{}^1S_0, F^g = 9/2, M_F^g = 9/2\rangle$ is given by

$$\begin{aligned} a(M_F^e, M_F^g)_{\text{HIT}} &= \frac{2.02613 \times 10^{18}}{\lambda^3} \sum_q | \langle {}^1S_0, F^g = 9/2, M_F^g = 9/2 | \mathbf{E}_q^{(1)} | {}^3P_0^e, F^e = 9/2, M_F^e = 9/2 \rangle |^2, \end{aligned} \quad (8)$$

where $\mathbf{E}_q^{(1)}$ is the q th component of the electric dipole transition operator $\mathbf{E}^{(1)}$ and λ is the transition wavelength in angstroms. By submitting Eqs. (6) and (7) into the above equation, the transition rate $a(M_F^e, M_F^g)_{\text{HIT}}$ between the excited

Zeeman state and the ground Zeeman state is then given as

$$a(M_F^e, M_F^g)_{\text{HIT}} = \frac{2.02613 \times 10^{18}}{\lambda^3} \sum_q \left| \sum_{s:F'} d_{s:F'} \right. \\ \times \sqrt{2F^g + 1} \sqrt{2F' + 1} \begin{pmatrix} F^g & 1 & F' \\ -M_F^g & q & M_F^e \end{pmatrix} \\ \left. \times \begin{Bmatrix} J^g & F^g & I \\ F' & J^e & 1 \end{Bmatrix} \langle ns^2 \ ^1S_0 | \mathbf{E}^{(1)} | nsnp \ ^sP_1^o \rangle \right|^2. \quad (9)$$

The total transition rate is obtained by

$$A(M_F^e)_{\text{HIT}} = \sum_{M_F^g} a(M_F^e, M_F^g)_{\text{HIT}} \\ = \frac{2.02613 \times 10^{18}}{3\lambda^3} \\ \times \left| \sum_s d_s \langle 5s^2 \ ^1S_0 | \mathbf{E}^{(1)} | 5s5p \ ^sP_1^o \rangle \right|^2, \quad (10)$$

where the dependence on the nuclear magnetic moment μ_I , electric quadrupole moment Q , nuclear spin I , F' , M_F^g , and B has been absorbed in the mixing coefficients d_s .

B. MCDHF method

According to the MCDHF method [45–48], the atomic state function $\Psi(\Gamma P J M_J)$ is a linear combination of a number of configuration state functions (CSFs) $\Phi_j(\gamma_j P J M_J)$ with the same parity P , total angular quantum number J , and magnetic quantum number M_J ,

$$\Psi(\Gamma P J M_J) = \sum_j^N c_j \Phi_j(\gamma_j P J M_J), \quad (11)$$

where c_j represents the configuration mixing coefficient and γ stands for the other quantum numbers that define the state uniquely. The configuration state functions $\Phi_j(\gamma_j P J M_J)$ are built from sums of products of one-electron Dirac orbitals. In the self-consistent field (SCF) procedure, the coefficients c_j and the radial functions of the one-electron Dirac orbitals are determined simultaneously by solving the MCDHF equations. The relativistic configuration interaction (RCI) procedure can consider higher-order electron correlations, the Breit interaction, and QED corrections, but it optimizes only the expansion coefficients. Once the wave functions of the atomic states have been obtained, the transition rate can be evaluated in terms of the reduced matrix element $\langle \Psi(PJ) \| \mathbf{O}^{(\lambda)} \| \Psi(P'J') \rangle$, where the tensor operator $\mathbf{O}^{(\lambda)}$ is a multipole radiation-field operator. The biorthogonal transformation technique [49,50] is used to compute the reduced-transition-matrix elements in which the even- and odd-parity wave functions are built from independently optimized orbital sets.

C. Computational method

Our calculations began with the Dirac-Hartree-Fock (DHF) calculation, which was used to optimize the spectroscopic orbitals occupied in reference configurations. The even and odd reference configurations were considered separately. The

outermost electrons, $5s$ and $5p$, in the reference configurations were treated as the valence electrons, and others were treated as the core. The configuration expansions were generated by single (S) and double (D) excitations from the reference configurations to an active set of orbitals. The valence-valence (VV) and core-valence (CV) correlations between the $n = 3$, 4 core shells and the valence electrons were considered in the SCF computational procedure. The SD excitations were restricted, so that at most one electron in the core subshell can be replaced with the active or virtual orbitals. Seven layers of virtual orbitals were augmented layer by layer to converge the parameters under investigation, and only the added orbitals were variable each time. In each step, the computational model was labeled C_3V-n , where n represents the largest principal quantum number in the orbital set.

Keeping all orbitals frozen, the effect of the CV correlation related to the $n \leq 2$ electrons was further considered in the subsequent RCI computation, whose computational model was labeled C_1V . The core-core (CC) correlation among the $n = 4$ core shell, labeled CC_4 , was also captured in the RCI. To control the number of CSFs, only the first five layers of virtual orbitals were used to generate the CSFs accounting for the CC correlation. Furthermore, the higher-order electron correlations among $n \geq 4$ electrons were taken into account by the multireference (MR) configuration SD excitation model. The MR configurations were formed by selecting the dominant configurations in the CC_4 configuration space. For the even and odd states, the MR configurations were composed of $\{4s^2 4p^6 5s^2, 4s^2 4p^6 5p^2, 4s^2 4p^5 4d 5s 5p, 4s^2 4p^6 5s 6s\}$ and $\{4s^2 4p^6 5s 5p, 4s^2 4p^6 4d 5p, 4s^2 4p^6 5s 6p, 4s^2 4p^6 5p 6s, 4s^2 4p^6 4d 6p\}$, respectively. The configuration space was expanded by SD-excitation CSFs from the MR configurations to the first five layers of virtual orbitals. Finally, the Breit interaction and QED correlations were evaluated based on the MR model. Our calculations were performed using the GRASP2K package [51].

D. Numerical results and discussion

As presented in Eq. (10), we obtained a formula for the hyperfine quenching rate. Using the nuclear spin $I = 9/2$, the nuclear magnetic dipole moment $\mu_I = -1.0936030(13)\mu_N$ [52], and the electric quadrupole moment $Q = 0.328(4)$ b [53], we calculated the off-diagonal reduced hyperfine interaction matrix elements W and the mixing coefficients d_s between the $^3P_0^o$ and perturbing states ($^3P_1^o$ and $^1P_1^o$). The calculated results as a function of computational models are presented in Table I. In Table I, the unit of the mixing coefficient d_s is transformed to the atomic unit by choosing $\mu_N = 1.987131 \times 10^{-6}$ [30]. With the calculated mixing coefficients and the reduced electric dipole matrix elements (in Babushkin gauge) between the ground state and the perturbing states, we obtained the hyperfine quenching rate and lifetime of the $^3P_0^o$ state. The calculated transition rates and lifetimes in different models are presented in the last two columns of Table I. From Table I, one can see that the VV and CV correlations make dominant contributions to the transition rate. The CC correlation is also important because it causes a 28% change in the transition rate. But the higher-order electron correlations counteract the CC correlation effects and make

TABLE I. The off-diagonal reduced hyperfine interaction matrix elements W (in a.u.) and the mixing coefficients d_s (in a.u.), along with the HIT rate A and the lifetime τ of the $5s5p \ ^3P_0^o$ state, from different computational models. The number in square brackets represents the power of 10.

Model	$(^3P_1^o, ^3P_0^o)$		$(^1P_1^o, ^3P_0^o)$		A (s^{-1})	τ (s)
	W_3	d_3	W_1	d_1		
DHF	-1.677[-7]	2.015[-4]	-1.218[-7]	1.745[-6]	1.43[-3]	699
C_3V-5	-1.053[-7]	1.945[-4]	-1.635[-7]	2.784[-6]	3.10[-3]	323
C_3V-6	-1.386[-7]	2.430[-4]	-1.932[-7]	3.846[-6]	7.71[-3]	130
C_3V-7	-1.453[-7]	2.631[-4]	-2.057[-7]	4.055[-6]	4.75[-3]	211
C_3V-8	-1.607[-7]	2.815[-4]	-2.207[-7]	4.476[-6]	8.94[-3]	112
C_3V-9	-1.605[-7]	2.843[-4]	-2.218[-7]	4.493[-6]	8.66[-3]	115
C_3V-10	-1.623[-7]	2.886[-4]	-2.235[-7]	4.546[-6]	8.86[-3]	113
C_3V-11	-1.618[-7]	2.879[-4]	-2.230[-7]	4.533[-6]	8.79[-3]	114
C_1V	-2.248[-7]	2.900[-4]	-1.636[-7]	4.584[-6]	8.96[-3]	112
CC4	-2.048[-7]	2.448[-4]	-1.534[-7]	3.072[-6]	4.20[-3]	238
MR	-2.016[-7]	2.333[-4]	-1.444[-7]	4.119[-6]	6.07[-3]	164
Breit+QED	-2.023[-7]	2.379[-4]	-1.450[-7]	4.144[-6]	6.21[-3]	161
Revised	-2.023[-7]	2.377[-4]	-1.450[-7]	4.315[-6]	6.39[-3]	156(9)
Other theories						
Pal'chikov [24]						183
Santra <i>et al.</i> [26]						110(30)
Porsev and Derevianko [27]						132
Boyd <i>et al.</i> [25]						145(40)
Other measurements						
Dörscher <i>et al.</i> [28]						330(140)
Muniz <i>et al.</i> [29]						118(3)

the results obtained in the MR model close to the ones in the C_1V model. Additionally, the Breit interaction and QED correlations contribute approximately 5% to the quenching rate.

In Ref. [53], we constructed different computational models which were labeled $C_{nl}V$ (nl represents the last opened core subshell) to analyze which core electrons strongly interact with the valence electrons for the eigenenergies and hyperfine structures of the $5s5p \ ^3P_{1,2}^o, \ ^1P_1^o$ states. Like for the $5s5p$ configuration, we also constructed different computational models to analyze the core electrons' and the valence electrons' correlation effects on the eigenenergy of the ground state. As spin polarization represents the major contribution to the hyperfine interaction, we analyzed the spin polarizations of different s subshells because the s electrons have high spin densities at the nucleus [54]. The spin polarization was included separately by CSFs of the form $1s^22s^22p^63s^23p^63d^{10}4s(ns)4p^6, 1s^22s^22p^63s(ns)3p^63d^{10}4s^24p^6, 1s^22s(ns)2p^63s^23p^63d^{10}4s^24p^6$, and $1s(ns)2s^22p^63s^23p^63d^{10}4s^24p^6$. For example, to consider the spin polarization from the $4s$ subshell, we added the $1s^22s^22p^63s^23p^63d^{10}4s(ns)4p^6$ CSFs to the $C_{4p}V$ configuration space, whose model was labeled $C_{4p}V + 4sSP$. The $4s$ spin-polarization effect was obtained from the difference in results between the $C_{4p}V + 4sSP$ model and the $C_{4p}V$ model. The spin polarizations of individual $3s, 2s$, and $1s$ orbitals were included in the same way. The contributions of the spin polarizations of $4s, 3s, 2s$, and $1s$ orbitals to the HIT rate are presented in Table II. From Table II, we can see that the spin-polarization effect of the $4s$ orbital on the HIT rate is much larger than that of other orbitals. The deeper orbitals

correspond to the smaller contributions to the HIT rate. The total spin-polarization effects make an about 28% contribution to the HIT rate, compared to the C_1V model which contains the core-valence correlation (spin- and orbital-polarization effects).

To estimate the calculation uncertainty, both the convergence method and the gauge method [55] were employed, resulting in individual errors of 4% and 6% for the transition rate, respectively. The largest error source was selected as the final uncertainty, yielding the final values of the HIT rate $A(M_F^e)_{\text{HIT}} = 6.21(37) \times 10^{-3} \text{ s}^{-1}$. Good agreement was found for the fine-structure splitting between the $^3P_0^o$ and $^3P_1^o$ states, but the energy interval between $^3P_0^o$ and $^1P_1^o$ deviates from the NIST Atomic Spectra Database by 4% [56]. To obtain a more precise value of the transition rate, we used the energy gaps from NIST and revised the transition rate $A(M_F^e)_{\text{HIT}} = 6.39(37) \times 10^{-3} \text{ s}^{-1}$ and the lifetime of the $^3P_0^o$ state $\tau = 156(9) \text{ s}$. We calculated the transition

TABLE II. The effects of spin polarization of $4s, 3s, 2s$, and $1s$ orbitals on the HIT rate A_{HIT} . The number in square brackets represents the power of 10.

Spin polarization	A_{HIT} (s^{-1})
$4s$	2.02[-3]
$3s$	5.10[-4]
$2s$	-3.00[-5]
$1s$	2.00[-5]
C_1V	8.96[-3]

energies and rates [57,58] between the ground state and the $5s5p\ ^3P_{0,1,2}^o$, $^1P_1^o$ states and the hyperfine interaction constants A and B [53] of the $5s5p\ ^3P_{1,2}^o$, $^1P_1^o$ states. Our previous results agree with the measurements, which indicates the quality of our calculations.

Table I also includes other experimental and theoretical results for comparison. Table I shows that our result is in agreement with the results obtained by Santra *et al.* [26] using an effective core calculation and by Boyd *et al.* [25] using the modified Breit-Wills theory. In experiment, Dörscher *et al.* [28] reported a decay rate $\Gamma_0 = 5.2(12) \times 10^{-3} \text{ s}^{-1}$ for the $^3P_0^o$ excited state by investigating scattering of lattice laser radiation in a strontium optical lattice clock. The BBR-induced transition rate was also estimated as $\Gamma_{\text{BBR}} = 2.23(14) \times 10^{-3} \text{ s}^{-1}$ at the temperature $T = 294.5(10) \text{ K}$ since atoms in the $^3P_0^o$ state can be pumped to the $5s4d\ ^3D_1$ state and decay to the ground state via the $^3P_1^o$ state, which significantly increases the $^3P_0^o$ -state lifetime measurements. This is similar to estimating the lifetime of the $5s5p\ ^3P_2^o$ state in ^{88}Sr [58,59]. After the BBR-induced decay rate was accurately estimated and removed, the natural lifetime of the $^3P_0^o$ state was finally determined to be 330(140) s, which is considerably larger than our value. Muniz *et al.* [29] also determined the lifetime of the $^3P_0^o$ state $\tau = 118(3) \text{ s}$ for ^{87}Sr in cavity QED with smaller uncertainty but neglected the BBR-induced transition effect. The two measurements are inconsistent within their uncertainties even though both results correct the BBR-induced decay rate. As presented in Ref. [28], the BBR quenching rate is

$$\Gamma_{\text{BBR}}(T) = \frac{3R_0R_1}{\tau(^3D_1)} \frac{1}{\exp(\hbar\omega/k_B T) - 1}, \quad (12)$$

where R_0 and R_1 are the branching ratios of spontaneous decay from the 3D_1 state to the $^3P_0^o$ and $^3P_1^o$ states, respectively. The lifetime of the 3D_1 state is $\tau(^3D_1) = 2.18(1) \mu\text{s}$ [39], and ω is the $^3P_0^o - ^3D_1$ transition frequency. The BBR quenching rate is $\Gamma_{\text{BBR}} = 2.16 \times 10^{-3} \text{ s}^{-1}$ at room temperature $T = 294 \text{ K}$. Therefore, the spontaneous decay of the $^3P_0^o$ state measured in Ref. [29] is $\Gamma_s = \Gamma_0 - \Gamma_{\text{BBR}} = 8.47 \times 10^{-3} - 2.16 \times 10^{-3} = 6.31 \times 10^{-3} \text{ s}^{-1}$, which is in excellent agreement with our result.

In the presence of an external magnetic field, the off-diagonal reduced matrix elements $\langle J||T^{(1)}||J' \rangle$ and $\langle J||N^{(1)} + \Delta N^{(1)}||J' \rangle$ were calculated using the HFSZEEMAN [44] package. The unit of the reduced matrix element $\langle J||N^{(1)} + \Delta N^{(1)}||J' \rangle$ was transformed to the atomic unit by a conversion factor of 2.353×10^5 . Using Eq. (9), we calculated the transition rates $a(M_F^e, M_F^g)$ from the excited Zeeman states to the ground Zeeman states with external magnetic field $B = 0, 100, \text{ and } 200 \text{ G}$. The calculated results are presented in Table III, along with the Einstein transition rate $A(M_F^e)$ and the corresponding lifetime of the “ $5s5p\ ^3P_0^o IF^e M_F^e$ ” state τ . As shown in Table III, the transition rates $a(M_F^e, M_F^g)$ for the same excited Zeeman state differ due to variations in the Clebsch-Gordan coefficient while the magnetic-field strength remains the same. Moreover, the transition rate for magnetic quantum number $M_F^e \geq 0$ decreases as magnetic-field strength increases, whereas the opposite is true for magnetic quantum number $M_F^e < 0$. The statistical averages of the magnetic sub-levels are $\tau = 156.49, 156.77, \text{ and } 157.39 \text{ s}$, indicating that

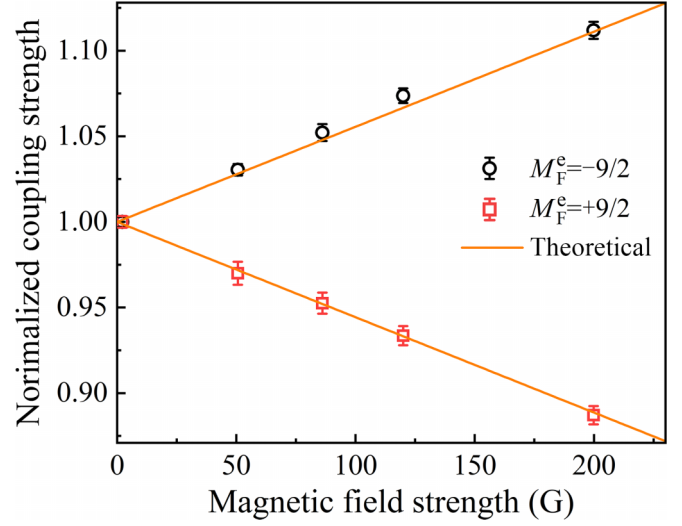


FIG. 3. The normalized coupling strength as a function of magnetic-field strength. The solid lines depict the theoretical calculations, while the error bars signify the experimental uncertainty within 1σ . In order to standardize the effective coupling strengths for both the theoretical calculations and experimental measurements, normalization is performed at a magnetic-field strength of 2.18 G.

the lifetime of the $^3P_0^o$ state is slightly affected by the weak magnetic field.

E. Comparison with the experimental measurements

In the ^{87}Sr optical lattice clock, the Rabi frequency of the clock transition from a specific M_F^e state is defined as

$$\Omega_{M_F^e}(B) = -\langle \langle 5s^2\ ^1S_0 IF^g = IM_F^g \rangle \langle \vec{d} | \langle 5s5p\ ^3P_0^o IF^e = IM_F^e \rangle \cdot \vec{E} / \hbar, \quad (13)$$

where $\langle \langle 5s^2\ ^1S_0 IF^g = IM_F^g \rangle \langle \vec{d} | \langle 5s5p\ ^3P_0^o IF^e = IM_F^e \rangle$ is the transition matrix element between the ground state and the excited state and \vec{E} represents the electric-field strength, which is directly related to the intensity of the clock laser. As per Eq. (10), it is evident that the matrix element is linearly dependent on the transition matrix elements between the 1S_0 state and $^1,^3P_1^o$ states. Additionally, the mixing coefficients exhibit linear relationships with the external magnetic-field intensity B . Hence, variations in the external magnetic field lead to changes in the Rabi frequency. Based on our aforementioned calculations, for $M_F^e = \pm 9/2$, the Rabi frequency defined in Eq. (13) is simplified as

$$\Omega_{M_F^e = \pm 9/2}(B) = (2.97 \times 10^{-5} \pm 1.64 \times 10^{-4} B) \cdot \vec{E} / \hbar. \quad (14)$$

Since the absolute value of the clock laser intensity is difficult to measure precisely in this work, we determined the theoretical calculations by keeping the clock laser intensity constant and measuring the normalized Rabi frequency $\tilde{\Omega} = \Omega_{M_F^e = \pm 9/2}(B) / \Omega_{M_F^e = \pm 9/2}(2.18)$ as a function of magnetic-field strength. The measured result is shown in Fig. 3 along with the theoretical calculations for comparison. From Fig. 3, we can see that our calculations perfectly agree with the measurements, indicating that the theoretical model and calculation results are correct.

TABLE III. Hyperfine-induced ${}^3P_0^o - {}^1S_0$ $E1$ transition rates in the presence of magnetic fields $B = 0$ G, $B = 100$ G, and $B = 200$ G for the ${}^{87}\text{Sr}$ isotope. a represents the transition rate from the excited state “ $5s5p {}^3P_0^o IF^e M_F^e$ ” to the ground state “ $5s^2 {}^1S_0 IF^g M_F^g$ ”. A represents the total transition rate from the excited state “ $5s5p {}^3P_0^o IF^e M_F^e$ ” to the ground states, and τ is the lifetime of the excited state.

M_F^e	M_F^g	ΔM	$B = 0$ G			$B = 100$ G			$B = 200$ G		
			a (s^{-1})	A (s^{-1})	τ (s)	a (s^{-1})	A (s^{-1})	τ (s)	a (s^{-1})	A (s^{-1})	τ (s)
9/2	9/2	0	5.23[-3]	6.39[-3]	156.49	4.67[-3]	5.83[-3]	171.53	4.14[-3]	5.30[-3]	188.68
	7/2	-1	1.16[-3]			1.16[-3]			1.16[-3]		
7/2	9/2	1	1.16[-3]	6.39[-3]	156.49	1.06[-3]	5.95[-3]	168.07	0.97[-3]	5.55[-3]	180.18
	7/2	0	3.16[-3]			2.80[-3]			2.47[-3]		
	5/2	-1	2.07[-3]			2.09[-3]			2.11[-3]		
5/2	7/2	1	2.07[-3]	6.39[-3]	156.49	1.91[-3]	6.08[-3]	164.47	1.76[-3]	5.79[-3]	172.71
	5/2	0	1.61[-3]			1.40[-3]			1.20[-3]		
	3/2	-1	2.71[-3]			2.77[-3]			2.83[-3]		
3/2	5/2	1	2.71[-3]	6.39[-3]	156.49	2.53[-3]	6.20[-3]	161.29	2.36[-3]	6.04[-3]	165.56
	3/2	0	0.58[-3]			0.47[-3]			0.37[-3]		
	1/2	-1	3.10[-3]			3.20[-3]			3.31[-3]		
1/2	3/2	1	3.10[-3]	6.39[-3]	156.49	2.93[-3]	6.33[-3]	157.98	2.76[-3]	6.29[-3]	158.98
	1/2	0	0.06[-3]			0.03[-3]			0.01[-3]		
	-1/2	-1	3.23[-3]			3.37[-3]			3.52[-3]		
-1/2	1/2	1	3.23[-3]	6.39[-3]	156.49	3.09[-3]	6.47[-3]	154.56	2.95[-3]	6.56[-3]	152.44
	-1/2	0	0.06[-3]			0.11[-3]			0.16[-3]		
	-3/2	-1	3.10[-3]			3.27[-3]			3.45[-3]		
-3/2	-1/2	1	3.10[-3]	6.39[-3]	156.49	3.00[-3]	6.59[-3]	151.75	2.90[-3]	6.82[-3]	146.63
	-3/2	0	0.58[-3]			0.70[-3]			0.84[-3]		
	-5/2	-1	2.71[-3]			2.89[-3]			3.08[-3]		
-5/2	-3/2	1	2.71[-3]	6.39[-3]	156.49	2.65[-3]	6.72[-3]	148.81	2.59[-3]	7.08[-3]	141.24
	-5/2	0	1.61[-3]			1.84[-3]			2.09[-3]		
	-7/2	-1	2.07[-3]			2.23[-3]			2.40[-3]		
-7/2	-5/2	1	2.07[-3]	6.39[-3]	156.49	2.04[-3]	6.85[-3]	145.99	2.02[-3]	7.35[-3]	136.05
	-7/2	0	3.16[-3]			3.54[-3]			3.95[-3]		
	-9/2	-1	1.16[-3]			1.27[-3]			1.38[-3]		
-9/2	-7/2	1	1.16[-3]	6.39[-3]	156.49	1.16[-3]	6.98[-3]	143.27	1.16[-3]	7.61[-3]	131.41
	-9/2	0	5.23[-3]			5.82[-3]			6.45[-3]		

IV. CONCLUSION

Using the MCDHF method, we calculated the lifetime of the $5s5p {}^3P_0^o$ clock state in ${}^{87}\text{Sr}$, and our result indicates a lifetime of 156(9) s. Our result agrees well with the most recent measurement that incorporated the BBR-induced transition correction. Additionally, we deduced the transition rates between the excited Zeeman and ground Zeeman states as a function of the magnetic-field strength. The theoretical result shows that the transition rates of the excited Zeeman states are highly influenced by weak external magnetic field, while their effects on the average lifetime of the ${}^3P_0^o$ state are negligible. This conclusion was supported by measuring the Rabi frequency as a function of external magnetic-field strength. Our work significantly improves the theoretical precision of the ${}^3P_0^o$ -state lifetime of ${}^{87}\text{Sr}$, resolves the discrepancy between theoretical and experimental data, and provides a foundation for studying the effect of external magnetic fields on hyperfine-induced transition rates of $nsnp {}^3P_0^o$ states and

corresponding Zeeman sublevels. Our results have many interesting applications, including the ability to easily measure the ${}^3P_0^o$ lifetime of ${}^{87}\text{Sr}$ by applying a strong external magnetic field to increase the decay rate, whereby the lifetime can be deduced from the excited-state decay rate. Additionally, the longer lifetime characteristic of a particular Zeeman sublevel in an external magnetic field may be useful in optical clocks in which the lifetime of the ${}^3P_0^o$ clock state is short, such as the ${}^{115}\text{In}^+$ optical clock [60], thereby improving clock stability and measurement precision.

ACKNOWLEDGMENTS

This work is supported by the National Natural Science Foundation of China (Grant No. 12203057), the Strategic Priority Research Program of the Chinese Academy of Sciences (Grant No. XDB35010202), and the Shaanxi Province Youth Science and Technology Star (Grant No. 2021KJXX-58).

[1] W. F. McGrew, X. Zhang, H. Leopardi, R. J. Fasano, D. Nicolodi, K. Bely, J. Yao, J. A. Sherman, S. A. Schäffer,

J. Savory, R. C. Brown, S. Römisch, C. W. Oates, T. E. Parker, T. M. Fortier, and A. D. Ludlow, *Optica* **6**, 448 (2019).

- [2] A. Aeppli, A. Chu, T. Bothwell, C. J. Kennedy, D. Kedar, P. He, A. M. Rey, and J. Ye, *Sci. Adv.* **8**, eadc9242 (2022).
- [3] X. T. Lu, T. Wang, T. Li, C. H. Zhou, M. J. Yin, Y. B. Wang, X. F. Zhang, and H. Chang, *Phys. Rev. Lett.* **127**, 033601 (2021).
- [4] M. J. Yin, X. T. Lu, T. Li, J. J. Xia, T. Wang, X. F. Zhang, and H. Chang, *Phys. Rev. Lett.* **128**, 073603 (2022).
- [5] X. Lu, J. Xia, B. Lu, Y. Wang, T. Wang, and H. Chang, *Appl. Phys. Lett.* **120**, 151104 (2022).
- [6] W. F. McGrew, X. Zhang, R. J. Fasano, S. A. Schäffer, K. Beloy, D. Nicolodi, R. C. Brown, N. Hinkley, G. Milani, M. Schioppo, T. H. Yoon, and A. D. Ludlow, *Nature (London)* **564**, 87 (2018).
- [7] E. Oelker, R. B. Hutson, C. J. Kennedy, L. Sonderhouse, T. Bothwell, A. Goban, D. Kedar, C. Sanner, J. M. Robinson, G. E. Marti, D. G. Matei, T. Legero, M. Giunta, R. Holzwarth, F. Riehle, U. Sterr, and J. Ye, *Nat. Photon.* **13**, 714 (2019).
- [8] R. Schwarz, S. Dörscher, A. Al-Masoudi, E. Benkler, T. Legero, U. Sterr, S. Weyers, J. Rahm, B. Lipphardt, and C. Lisdat, *Phys. Rev. Res.* **2**, 033242 (2020).
- [9] H. Kim, M.-S. Heo, C. Y. Park, D.-H. Yu, and W.-K. Lee, *Metrologia* **58**, 055007 (2021).
- [10] H. Hachisu, F. Nakagawa, Y. Hanado, and T. Ido, *Sci. Rep.* **8**, 4243 (2018).
- [11] T. Bothwell, C. J. Kennedy, A. Aeppli, D. Kedar, J. M. Robinson, E. Oelker, A. Staron, and J. Ye, *Nature (London)* **602**, 420 (2022).
- [12] M. Takamoto, I. Ushijima, N. Ohmae, T. Yahagi, K. Kokado, H. Shinkai, and H. Katori, *Nat. Photon.* **14**, 411 (2020).
- [13] K. Beloy *et al.*, *Nature (London)* **591**, 564 (2021).
- [14] M. S. Safronova, S. G. Porsev, C. Sanner, and J. Ye, *Phys. Rev. Lett.* **120**, 173001 (2018).
- [15] J.-P. Uzan, *Rev. Mod. Phys.* **75**, 403 (2003).
- [16] H. Miyake, N. C. Pisenti, P. K. Elgee, A. Sitaram, and G. K. Campbell, *Phys. Rev. Res.* **1**, 033113 (2019).
- [17] B. Lu, Y. Wang, Y. Guo, Q. Xu, M. Yin, J. Li, and H. Chang, *Chin. Phys. Lett.* **35**, 043203 (2018).
- [18] A. Goban, R. B. Hutson, G. E. Marti, S. L. Campbell, M. A. Perlin, P. S. Julienne, J. P. D’Incao, A. M. Rey, and J. Ye, *Nature (London)* **563**, 369 (2018).
- [19] T. Brage, M. Andersson, and R. Hutton, *ICAMDATA-2008: Sixth International Conference on Molecular Data and Their Applications*, AIP Conf. Proc. No. 1125 (AIP, Melville, NY, 2009), p. 18.
- [20] J. Grumer, T. Brage, M. Andersson, J. Li, P. Jönsson, W. Li, Y. Yang, R. Hutton, and Y. Zou, *Phys. Scr.* **89**, 114002 (2014).
- [21] M. Andersson, *Phys. Scr.* **T134**, 014021 (2009).
- [22] W. R. Johnson, *Can. J. Phys.* **89**, 429 (2011).
- [23] T. Brage, P. G. Judge, A. Aboussaïd, M. R. Godefroid, P. Jönsson, A. Ynnerman, C. Froese Fischer, and D. S. Leckrone, *Astrophys. J.* **500**, 507 (1998).
- [24] V. G. Pal’chikov, *16th European Frequency and Time Forum* (St. Petersburg State University of Aerospace Instrumentation, St. Petersburg, Rosja, 2002), p. E-002.
- [25] M. M. Boyd, T. Zelevinsky, A. D. Ludlow, S. Blatt, T. Zanon-Willette, S. M. Foreman, and J. Ye, *Phys. Rev. A* **76**, 022510 (2007).
- [26] R. Santra, K. V. Christ, and C. H. Greene, *Phys. Rev. A* **69**, 042510 (2004).
- [27] S. G. Porsev and A. Derevianko, *Phys. Rev. A* **69**, 042506 (2004).
- [28] S. Dörscher, R. Schwarz, A. Al-Masoudi, S. Falke, U. Sterr, and C. Lisdat, *Phys. Rev. A* **97**, 063419 (2018).
- [29] J. A. Muniz, D. J. Young, J. R. K. Cline, and J. K. Thompson, *Phys. Rev. Res.* **3**, 023152 (2021).
- [30] K. T. Cheng, M. H. Chen, and W. R. Johnson, *Phys. Rev. A* **77**, 052504 (2008).
- [31] M. Andersson, Y. Zou, R. Hutton, and T. Brage, *Phys. Rev. A* **79**, 032501 (2009).
- [32] S. Schippers, D. Bernhardt, A. Müller, M. Lestinsky, M. Hahn, O. Novotný, D. W. Savin, M. Grieser, C. Krantz, R. Repnow, and A. Wolf, *Phys. Rev. A* **85**, 012513 (2012).
- [33] W. Li, P. Jönsson, T. Brage, and R. Hutton, *Phys. Rev. A* **96**, 052508 (2017).
- [34] J. Li and C. Dong, *Plasma Sci. Technol.* **12**, 364 (2010).
- [35] S. Schippers, E. W. Schmidt, D. Bernhardt, D. Yu, A. Müller, M. Lestinsky, D. A. Orlov, M. Grieser, R. Repnow, and A. Wolf, *Phys. Rev. Lett.* **98**, 033001 (2007).
- [36] J. Li, C. Dong, P. Jönsson, and G. Gaigalas, M_F -dependent hyperfine induced transition rates in an external magnetic field for Be-like $^{47}\text{Ti}^{18+}$, *Phys. Lett. A* **375**, 914 (2011).
- [37] B. J. Bloom, T. L. Nicholson, J. R. Williams, S. L. Campbell, M. Bishof, X. Zhang, W. Zhang, S. L. Bromley, and J. Ye, *Nat. Commun.* **506**, 5 (2015).
- [38] I. Ushijima, M. Takamoto, M. Das, T. Ohkubo, and H. Katori, *Nat. Photon.* **9**, 185 (2015).
- [39] T. L. Nicholson, S. L. Campbell, R. B. Hutson, G. E. Marti, B. J. Bloom, R. L. McNally, W. Zhang, M. D. Barrett, M. S. Safronova, G. F. Strouse, W. L. Tew, and J. Ye, *Nat. Commun.* **6**, 6896 (2015).
- [40] Y. Wang, M. Yin, J. Ren, Q. Xu, B. Lu, J. Han, Y. Guo, and H. Chang, *Chin. Phys. B* **27**, 023701 (2018).
- [41] X. Lu, F. Guo, Y. Wang, Q. Xu, C. Zhou, J. Xia, W. Wu, and H. Chang, *Metrologia* **60**, 015008 (2023).
- [42] S. Blatt, J. W. Thomsen, G. K. Campbell, A. D. Ludlow, M. D. Swallows, M. J. Martin, M. M. Boyd, and J. Ye, *Phys. Rev. A* **80**, 052703 (2009).
- [43] C. Schwartz, *Phys. Rev.* **97**, 380 (1955).
- [44] M. Andersson and P. Jönsson, *Comput. Phys. Commun.* **178**, 156 (2008).
- [45] C. Froese Fischer, T. Brage, and P. Jönsson, *Computational Atomic Structure: An MCHF Approach* (Institute of Physics Publishing, London, 1997).
- [46] J. Bieroń, C. Froese Fischer, S. Fritzsche, G. Gaigalas, I. P. Grant, P. Indelicato, P. Jönsson, and P. Pyykkö, *Phys. Scr.* **90**, 054011 (2015).
- [47] C. F. Fischer, M. Godefroid, T. Brage, P. Jönsson, and G. Gaigalas, *J. Phys. B* **49**, 182004 (2016).
- [48] P. Jönsson, G. Gaigalas, C. F. Fischer, J. Bieroń, I. P. Grant, T. Brage, J. Ekman, M. Godefroid, J. Grumer, J. Li, and W. Li, *Atoms* **11**, 68 (2023).
- [49] J. Olsen, M. R. Godefroid, P. Jönsson, P. A. Malmqvist, and C. F. Fischer, *Phys. Rev. E* **52**, 4499 (1995).
- [50] S. Verdebout, P. Jönsson, G. Gaigalas, M. Godefroid, and C. Froese Fischer, *J. Phys. B* **43**, 074017 (2010).
- [51] P. Jönsson, G. Gaigalas, J. Bieroń, C. Froese Fischer, and I. P. Grant, *Comput. Phys. Commun.* **184**, 2197 (2013).
- [52] J. E. Sansonetti and G. Nave, *J. Phys. Chem. Ref. Data* **39**, 033103 (2010).

- [53] B. Lu, T. Zhang, H. Chang, J. Li, Y. Wu, and J. Wang, *Phys. Rev. A* **100**, 012504 (2019).
- [54] Y. Liu, R. Hutton, Y. Zou, M. Andersson, and T. Brage, *J. Phys. B* **39**, 3147 (2006).
- [55] M. Andersson, Y. Liu, C. Y. Chen, R. Hutton, Y. Zou, and T. Brage, *Phys. Rev. A* **78**, 062505 (2008).
- [56] A. Kramida, Yu. Ralchenko, J. Reader, and NIST ASD Team, NIST Atomic Spectra Database, version 5.10, <https://physics.nist.gov/asd>.
- [57] B. Lu, Y. Wang, J. Han, S. Zhang, J. Li, and H. Chang, *J. Phys. Commun.* **1**, 055017 (2017).
- [58] B. Lu, X. Lu, J. Li, and H. Chang, *Chin. Phys. Lett.* **39**, 073201 (2022).
- [59] M. Yasuda and H. Katori, *Phys. Rev. Lett.* **92**, 153004 (2004).
- [60] N. Ohtsubo, Y. Li, N. Nemitz, H. Hachisu, K. Matsubara, T. Ido, and K. Hayasaka, *Opt. Lett.* **45**, 5950 (2020).

Correction: Reference [36] and its citations in Secs. I and III A were missing and have been inserted. Subsequent references have been renumbered. The author names in Ref. [34] were presented incorrectly and have been fixed.